






Electron transitions for Dirac Hamiltonians with flat bands under electromagnetic radiation: Application to the $\alpha - \mathcal{T}_3$ graphene model

M. A. Mojarro ¹, V. G. Ibarra-Sierra ^{2,*}, J. C. Sandoval-Santana ³, R. Carrillo-Bastos ¹ and Gerardo G. Naumis ²

¹Facultad de Ciencias, Universidad Autónoma de Baja California, Apartado Postal 1880, 22800 Ensenada, Baja California, México

²Departamento de Sistemas Complejos, Instituto de Física, Universidad Nacional Autónoma de México, Apartado Postal 20-364, 01000, Ciudad de México, México

³Instituto de Física, Universidad Nacional Autónoma de México, Apartado Postal 20-364, 01000, Ciudad de México, México



(Received 2 February 2020; accepted 25 March 2020; published 15 April 2020)

In a system with a Dirac-like linear dispersion there are always states that fulfill the resonance condition for electromagnetic radiation of arbitrary frequency Ω . When a flat band is present, two coexistent kinds of resonant transitions are found. Considering the $\alpha - \mathcal{T}_3$ graphene model as a minimal model with a flat band and Dirac cones and describing the dynamics using the interaction picture, we study the band transitions induced by an external electromagnetic field. We find that transitions depend upon the relative angle between the electron momentum and the electromagnetic field wave vector. For parallel incidence, the transitions are found using Floquet theory, while for other angles perturbation theory is used. In all cases, the transition probabilities and the frequencies are found. For the parallel momentum, no symmetry is broken by the field, and light does not change the spectrum, while for some limit special cases of the parameter α or by charge doping, the system behaves as a three-level or two-level Rabi system. All these previous results were compared with numerical simulations. Good agreement was found between both. The obtained results show a rich system in which different kinds of transitions coexist.

DOI: [10.1103/PhysRevB.101.165305](https://doi.org/10.1103/PhysRevB.101.165305)

I. INTRODUCTION

Following the recent discovery of correlated insulation and avowedly unconventional superconductivity in twisted bilayer graphene [1], the interest in the physics related to this system, in particular in the flat bands that appear at the so-called magic angles [2], has rapidly grown [3]. Remarkable effects are seen in the optical properties by twisting bilayer graphene; for example, Van Hove singularities lead to an energy band gap lying in the visible spectrum of electromagnetic radiation [3]. Such a gap is absent in any other known form of graphene [3]. Although many studies are devoted to understanding how flat bands arise in Dirac systems [4,5] and how they produce diverse quantum phases [6,7], still, the effects of electromagnetic radiation are not well understood. Happily, a minimal model that also presents flat bands coexisting with Dirac cone states is the $\alpha - \mathcal{T}_3$ model, which consists of a honeycomb lattice with an additional atom located at the center of each hexagon and coupled to the atoms of just one of the two nonequivalent sublattices [8–12]. While in twisted bilayer graphene the flat band arises at magic angles due to the multiple band crossings from the folding of the Brillouin zone caused by the moiré pattern [2,5], in the $\alpha - \mathcal{T}_3$ model the flat band comes from the local topology in the lattice [9].

There are several achievable experimental systems that can be mapped to a low-energy $\alpha - \mathcal{T}_3$ model. These include the $\text{Hg}_{1-x}\text{Cd}_x$ quantum well [13], the trilayer of cubic

lattices [14], and optical lattices [15]. The $\alpha - \mathcal{T}_3$ model takes its name from the parameter α , which stands for the coupling between sublattices; this parameter continuously changes the system from one with just two sublattices interacting (graphene plus a disconnected site) to one with the three sublattices equally coupled (dice lattice). Surprisingly enough, the dispersion relation for this system is α independent [16]. Nevertheless, breaking the symmetries in the system makes the physical quantities α dependent: introducing a potential barrier (breaking the spatial symmetry) results in an α -dependent transmission [17]; introducing a perpendicular magnetic field (breaking the time-reversal symmetry) makes the magneto-optical conductivity and the Hofstadter butterfly α dependent [18–22]. In general, for the $\alpha - \mathcal{T}_3$ model, the flat band and the value of α become relevant in the presence of electromagnetic fields. For example, the orbital susceptibility [23,24] can be tuned with the parameter α , and in contrast with graphene the plasmon branch is pinched to a single point [25]. Also, a recent study analyzed the topological characteristics in this structure under circularly polarized light. The model describes a Haldane-like Chern insulator characterized by a nonzero Chern number [26]. Therefore, the $\alpha - \mathcal{T}_3$ model undergoes a topological phase transition for Chern numbers from 1 to 2 in the valence band and from -1 to -2 in the conduction band at $\alpha = 1/\sqrt{2}$. More recently, it was found that this kind of Hamiltonian leads to an unexpected family of in-gap chiral edge states for noninverted spin-1 Dirac quantum dots [27]. There are some other previous works concerning the structure of the electromagnetic-dressed electron spectrum [26,28,29]. These

*vickkun@fisica.unam.mx

results indicate the opening of Floquet-band gaps, as has been determined before for other two-dimensional materials such as graphene [30–33] and borophene [34,35]. This is essential to calculate photocurrents [30], which is the usual way to experimentally test the dynamic Floquet bands [36,37] and other optical properties [38,39]. Also, there are relevant works that study the importance of the role of periodically driven time-dependent Rashba spin-orbit coupling on a monolayer of graphene [40,41]. For Dirac Hamiltonians with a flat band and under time-driven polarized light, the tight-binding model for the kagome lattice has also been studied [42,43]. However, a study of the transitions induced by time-driven electromagnetic fields is not available. In this work we present such a study. Especially, we show how the inclusion of flat-band states shares many similarities with the three-level Rabi problem [44], in which the flat band provides an intermediate step to mediate transitions from the valence to the conduction band. Our results show many useful relationships between transition probabilities, times, and parameters of the model. This can serve to combine experimental and theoretical results to fine-tune the parameters of the Hamiltonian, which is a problem that is still a work in progress [45], as well as a tool to have quantum control of the system.

The layout of this work is the following. In Sec. II we present the model and basic equations, while in Sec. III we include the electromagnetic field. Then in Sec. IV we identify the transitions and relevant features of the model. Section V is devoted to presenting the numerical results, and a discussion is undertaken to identify the relevant features of the model. Finally, in Sec. VI the conclusions are given.

II. HAMILTONIAN FOR THE $\alpha - \mathcal{T}_3$ MODEL

In the tight-binding low-energy approximation, the $\alpha - \mathcal{T}_3$ Hamiltonian model considering only nearest-neighbor hopping is given by [23–26,28,29]

$$\hat{H} = \begin{pmatrix} 0 & tC_\alpha f(\mathbf{k}) & 0 \\ tC_\alpha f^*(\mathbf{k}) & 0 & tS_\alpha f(\mathbf{k}) \\ 0 & tS_\alpha f^*(\mathbf{k}) & 0 \end{pmatrix}, \quad (1)$$

where $f(\mathbf{k}) = \sum_{i=1}^3 e^{-ik \cdot \delta_i}$ and t is the nearest-neighbor hopping amplitude, with δ_i ($i = 1, 2, 3$) being the vectors connecting the nearest-neighbor sites and $\mathbf{k} = (k_x, k_y)$ being the momentum vector.

It is important to remark here that, in principle, one needs to use the full tight-binding Hamiltonian to explore other sections of the Brillouin zone which are not close to the low-energy region. According to our experience [46–48], in general, one can expect different band crossings and even new kinds of topological states [49] at such zones, as seen recently in graphene with time-dependent strain [48]. However, probing such regions from an experimental point of view is challenging due to the intense fields required. Thus, here we concentrate on the most accessible part of the Brillouin zone and leave for future works the research of the full Brillouin zone.

The low-energy Hamiltonian around the two inequivalent Dirac points can be written as [25,28]

$$\hat{H}_\xi^0 = \hbar v_F \mathbf{k} \cdot \hat{\mathbf{S}}, \quad (2)$$

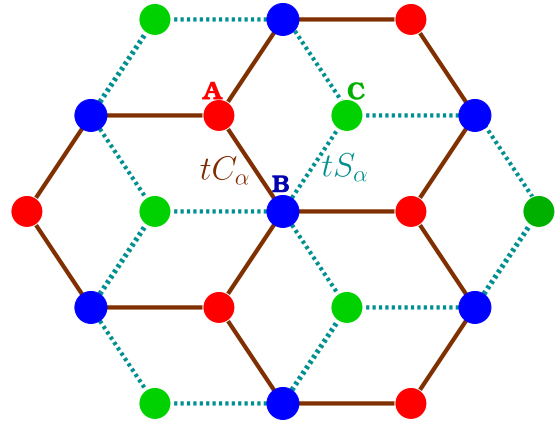


FIG. 1. Sketch of the $\alpha - \mathcal{T}_3$ lattice. When $\alpha = 0$, ($C_\alpha = 1$, $S_\alpha = 0$) results in the honeycomb lattice resembling monolayer graphene. In contrast, for $\alpha = 1$, ($C_\alpha = S_\alpha = 1/\sqrt{2}$) leads to the well-studied dice lattice with pseudospin 1 [25].

where $v_F \approx 10^6$ m/s is the Fermi velocity and $\hat{\mathbf{S}} = (\xi \hat{S}_x, \hat{S}_y)$, with $\xi = \pm 1$, refers to the \mathbf{K} and \mathbf{K}' valleys. The pseudospin operators \hat{S}_x and \hat{S}_y are defined as

$$\hat{S}_x = \begin{pmatrix} 0 & C_\alpha & 0 \\ C_\alpha & 0 & S_\alpha \\ 0 & S_\alpha & 0 \end{pmatrix}, \quad (3)$$

$$\hat{S}_y = \begin{pmatrix} 0 & -iC_\alpha & 0 \\ iC_\alpha & 0 & -iS_\alpha \\ 0 & iS_\alpha & 0 \end{pmatrix}, \quad (4)$$

with $C_\alpha = 1/\sqrt{1+\alpha^2}$, $S_\alpha = \alpha/\sqrt{1+\alpha^2}$, and $0 \leq \alpha \leq 1$. From Eq. (1) it is possible to find the electronic band structure and the eigenfunctions by solving the eigenvalue problem

$$\hat{H}_\xi^0 |\psi_{\mathbf{k},\mu}\rangle = E_\mu |\psi_{\mathbf{k},\mu}\rangle, \quad (5)$$

where the band structure consists of two Dirac cones and an additional flat band. The first cone is described by $E_1 = -v_F \hbar |\mathbf{k}|$, which corresponds to the valence band (VB); the flat band (FB) is described by $E_2 = 0$, and the second cone is $E_3 = v_F \hbar |\mathbf{k}|$ and describes the conduction band (CB). In Fig. 2, we show this band structure near the Dirac point \mathbf{K} ($\xi = +1$).

The eigenfunctions for each band are given by

$$|\psi_{\mathbf{k},1}\rangle = \frac{1}{\sqrt{2}} [\xi C_\alpha e^{-i\xi\theta_k} |A\rangle - |B\rangle + \xi S_\alpha e^{i\xi\theta_k} |C\rangle], \quad (6)$$

$$|\psi_{\mathbf{k},2}\rangle = \xi S_\alpha e^{-i\xi\theta_k} |A\rangle - \xi C_\alpha e^{i\xi\theta_k} |C\rangle, \quad (7)$$

$$|\psi_{\mathbf{k},3}\rangle = \frac{1}{\sqrt{2}} [\xi C_\alpha e^{-i\xi\theta_k} |A\rangle + |B\rangle + \xi S_\alpha e^{i\xi\theta_k} |C\rangle], \quad (8)$$

where $\theta_k = \tan^{-1}(k_y/k_x)$ and

$$|A\rangle = \begin{pmatrix} 1 \\ 0 \\ 0 \end{pmatrix}, \quad |B\rangle = \begin{pmatrix} 0 \\ 1 \\ 0 \end{pmatrix}, \quad |C\rangle = \begin{pmatrix} 0 \\ 0 \\ 1 \end{pmatrix}, \quad (9)$$

are the spinors that describe the sublattice degree of freedom (A, B, and C) in the unit cell, as shown in Fig. 1.

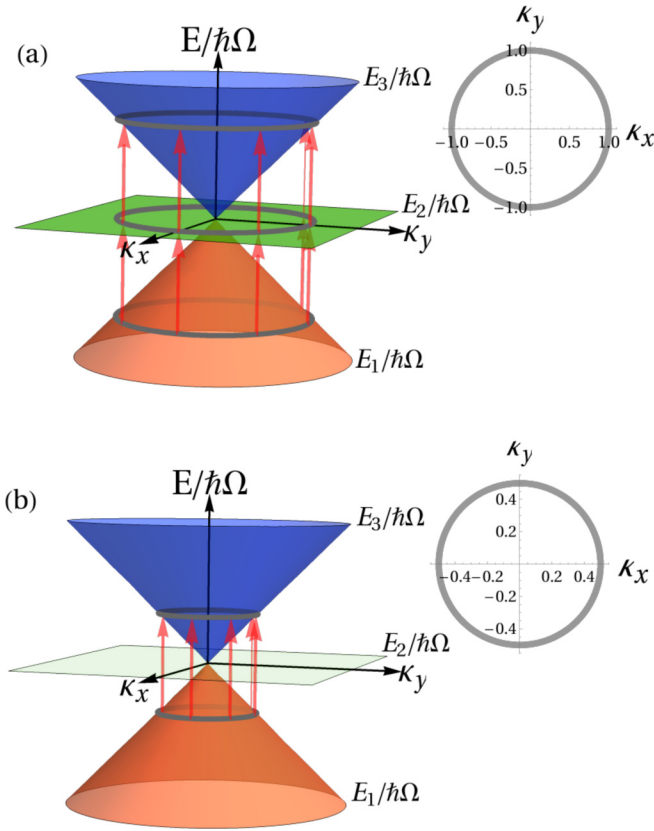


FIG. 2. Band structure of the $\alpha - \mathcal{T}_3$ lattice around the Dirac point \mathbf{K} . The light-blue Dirac cone corresponds to the CB (E_3), light green shows the FB (E_2), and light orange shows the VB (E_1). When an electromagnetic field with a given constant frequency Ω is introduced, direct interband transitions denoted by light-red arrows are allowed. (a) shows the transitions for the resonant frequency $\omega \approx \Omega$ (corresponding to $\kappa_x^2 + \kappa_y^2 \approx 1$, as indicated by the gray circle), which is associated with two simultaneous transitions from the VB to the FB and from the FB to the CB. In (b), we show the transition for the resonant frequency $\omega \approx \Omega/2$ (corresponding to $\kappa_x^2 + \kappa_y^2 \approx 1/4$, as indicated by the gray circle), which is associated with the transitions from the VB to the CB.

III. THE $\alpha - \mathcal{T}_3$ MODEL UNDER ELECTROMAGNETIC RADIATION AND THE INTERACTION PICTURE

To study the dynamics of the electrons in the $\alpha - \mathcal{T}_3$ model under electromagnetic radiation, we introduce a minimal coupling through the Peierls substitution [28] $\hbar\mathbf{k} \rightarrow \hbar\mathbf{k} - e\mathbf{A}$ in the low-energy Hamiltonian (2), where $\mathbf{A} = (A_x, A_y)$ is the vector potential of the electromagnetic wave. For this problem, we consider a gauge in which the components A_x and A_y are only a function of time.

From Eq. (2) we obtain

$$\hat{H}_\xi(t) = \hat{H}_\xi^0 + \hat{V}_\xi(t), \quad (10)$$

where \hat{H}_ξ^0 is given by Eq. (2) and $\hat{V}_\xi(t)$ is defined as

$$\hat{V}_\xi(t) = -ev_F\mathbf{A} \cdot \hat{\mathcal{S}}. \quad (11)$$

In Eqs. (2) and (11) the vectors $\hbar v_F \mathbf{k}$ and $ev_F \mathbf{A}$ represent the directional energy flux of electrons and the work done

by the electromagnetic wave along the x and y directions, respectively.

In the interaction picture [50], the Dirac equation for the $\alpha - \mathcal{T}_3$ model is given by

$$i\hbar \frac{d}{dt} \chi(t) = \mathbb{V}(t) \chi(t), \quad (12)$$

where the vector $\chi(t) = (\chi_1(t), \chi_2(t), \chi_3(t))^T$ contains the components of the wave functions in the VB ($\mu = 1$), FB ($\mu = 2$), and CB ($\mu = 3$) in the interaction picture and they are given by

$$\chi_\mu(t) = \exp\left[i\frac{E_\mu}{\hbar}t\right] \langle \psi_{\mathbf{k},\mu} | \Psi(t) \rangle \quad (13)$$

and $|\Psi(t)\rangle$ is a time-dependent three-component spinor in the Schrödinger picture. In Eq. (12), $\mathbb{V}(t)$ is a square matrix with dimensions 3×3 , and its components are defined as

$$[\mathbb{V}(t)]_{\mu,\nu} = \exp\left[i\frac{(E_\mu - E_\nu)}{\hbar}t\right] \langle \psi_{\mathbf{k},\mu} | \hat{V}_\xi(t) | \psi_{\mathbf{k},\nu} \rangle, \quad (14)$$

where the subindices $\mu, \nu = 1, 2, 3$ refer to the band.

Let us now study the case of a linearly polarized electromagnetic wave defined by the vector potential

$$\mathbf{A} = \frac{E_0}{\Omega} \cos(\Omega t) \hat{\mathbf{r}}, \quad (15)$$

where $\hat{\mathbf{r}} = (\cos \Theta, \sin \Theta)$ is the polarization vector, E_0 is the amplitude of the electric field, taken as constant, and Ω is the frequency of the electromagnetic wave. Notice that here we consider a classical field, and thus, we are assuming a quantum coherent field with a huge number of photons [51]. Without any loss of generality, we can take $\Theta = 0$ as the physics depending only upon the angle between Θ and θ_k .

Using Eq. (15) and rewriting Eqs. (12)–(14), we obtain

$$i\chi'(t) + \cos(\Omega t) \mathbb{B}(t) \chi(t) = 0, \quad (16)$$

where $\mathbb{B}(t)$ is a matrix defined as

$$\mathbb{B}(t) = \begin{pmatrix} -\epsilon & w e^{-i\omega t} & s e^{-i2\omega t} \\ w^* e^{i\omega t} & 0 & w e^{-i\omega t} \\ s^* e^{2i\omega t} & w^* e^{i\omega t} & \epsilon \end{pmatrix}. \quad (17)$$

The coefficients ϵ , w , and s from the previous expression are defined as

$$\epsilon = \zeta \cos \theta_k, \quad (18)$$

$$w = i\sqrt{2}\xi \mathcal{C}_\alpha \mathcal{S}_\alpha \zeta \sin \theta_k, \quad (19)$$

$$s = i\xi (\mathcal{C}_\alpha^2 - \mathcal{S}_\alpha^2) \zeta \sin \theta_k, \quad (20)$$

and the coefficient

$$\zeta = \frac{ev_F E_0}{\hbar \Omega}. \quad (21)$$

In Eq. (17) we used a set of renormalized moments, $\kappa_x = (v_F/\Omega)k_x$ and $\kappa_y = (v_F/\Omega)k_y$, which are related to ω as follows: $\omega = \Omega \sqrt{\kappa_x^2 + \kappa_y^2}$.

IV. TRANSITIONS

This section is devoted to studying the transitions that are obtained from Eq. (16). The first observation concerning Eq. (16) is that the system depends upon the angle θ_k . For some angles, the solutions of Eq. (16) are readily found by direct integration, while others require perturbation theory, as detailed below.

It is important to remark that previous works have shown that many-body systems with local interactions under external periodical driving can increase system's temperature [52–55]. However, the energy absorption rate decays exponentially as a function of the driving frequency and implies that many-body states in periodically driven systems, although metastable, can have very long lifetimes [52]. Here we do not consider such many-body effects, which certainly are important in correlated quantum phases.

A. Parallel or antiparallel incidence angle

When the electron momentum is parallel to the electric field, i.e., for $\theta_k = 0$ (also for the antiparallel $\theta_k = \pi$ the solution is similar), we have $w = 0$ and $s = 0$. Therefore, we have, in principle, that for $\eta = 1, 3$,

$$\chi_\eta(t) = \chi_\eta(0) \exp \left[\mp i \frac{\zeta}{\Omega} \sin(\Omega t) \right], \quad (22)$$

where the upper sign is for $\eta = 1$ and the lower sign is for $\eta = 3$. We also have $\chi_2(t) = \chi_2(0)$. Using Eq. (13), we obtain for $\eta = 1, 3$,

$$\langle \psi_{k,\eta} | \Psi(t) \rangle = \chi_\eta(0) \exp \left[\mp i \frac{\zeta}{\Omega} \sin \Omega t \right] \exp \left[-i \frac{E_\eta}{\hbar} t \right], \quad (23)$$

while for the flat band,

$$\langle \psi_{k,2} | \Psi(t) \rangle = \chi_2(0) \exp \left[-i \frac{E_2}{\hbar} t \right]. \quad (24)$$

Equations (23) and (24) show that band occupation probabilities are constant over time.

It is interesting to use Floquet theory to analyze such a result. We decompose Eq. (23) as a Fourier series,

$$\begin{aligned} \langle \psi_{k,\eta} | \Psi(t) \rangle &= \chi_\eta(0) \sum_{m=1}^{\infty} (-i)^m J_m \left(\frac{\zeta}{\Omega} \right) \exp \left[-\frac{i}{\hbar} (E_\eta + m\hbar\Omega)t \right], \end{aligned} \quad (25)$$

where $J_m(x)$ denotes the m -esim Bessel function. The argument of the exponential can be identified with the Floquet quasienergy $\epsilon_m = E_\eta + m\hbar\Omega$, with the first Brillouin zone determined by $\hbar\Omega$. Here $|J_m(\zeta/\Omega)|^2$ represents the amplitude of emission or absorption for $m = 1, 2, 3, 4, \dots$ photon processes starting from a coherent field, i.e., a field in which there is a huge number of photons present [51]. It is surprising to have photon emission and absorption while keeping the occupation probabilities the same. However, this is easy to understand if we observe that after a time period given by $T = 2\pi/\Omega$, the wave function only gets a phase given by

$$\langle \psi_{k,\eta} | \Psi(t + T) \rangle = \exp \left[\frac{2i\pi}{\hbar\Omega} \right] \langle \psi_{k,\eta} | \Psi(t) \rangle. \quad (26)$$

When the field is at resonance with a given E_μ , say, $E_1 = n\hbar\Omega$, with n being an integer, the change in phase in Eq. (26) is $2\pi n$ for $\eta = 1$ and $-2\pi n$ for $\eta = 3$. All these results are explained by the fact that the field does not break the symmetry along the x axis for this incidence. As we will see below, this is not the case for other incidence angles. It is important to add that the persistence of this symmetry classifies the system with linearly polarized light as topologically different from the case of circularly polarized light. In the former case no gap is opened by light, while in the latter a gap is open [26].

B. General incidence angle: Time-dependent perturbation theory

Obtaining an analytical solution for the system of equations that arises from Eq. (16) for $\theta_k \neq 0$ or $\theta_k \neq \pi$ is difficult. Nevertheless, it is possible to find information on the dynamics of $\alpha - \mathcal{T}_3$ in the interaction picture using time-dependent perturbation theory [50].

In this approach, the solution for each component of Eq. (16) can be expressed as follows:

$$\chi_\mu(t) = \chi_\mu^{(0)}(t) + \chi_\mu^{(1)}(t) + \dots, \quad (27)$$

where $\chi_\mu^{(0)}(t)$ and $\chi_\mu^{(1)}(t)$ signify amplitudes of zero order, first order, and so on, in the strength parameter ζ of the time-dependent potential.

To zero order the amplitudes are time independent,

$$\chi_\mu^{(0)} = \sum_\nu \langle \psi_{k,\mu} | \psi_{k,\nu} \rangle = \sum_\nu \delta_{\mu,\nu}, \quad (28)$$

where $|\psi_{k,\nu}\rangle$ denotes the initial state ν . The first-order correction is

$$\chi_\mu^{(1)}(t) = \sum_\nu a_{\mu\nu}(t), \quad (29)$$

where $a_{\mu\nu}(t)$ is given by

$$a_{\mu\nu}(t) = -|B_{\mu\nu}| \int_0^t e^{i \arg[B_{\mu\nu}(t')]} \cos(\Omega t') dt', \quad (30)$$

with $B_{\mu,\nu}$ being the coefficients defined in Eq. (17). For the transitions from the VB ($\mu = 1$) to the FB ($\nu = 2$) we obtain

$$\begin{aligned} a_{21}(t) &= -\frac{i\omega}{2} \left\{ \frac{1 - \exp[i(\omega + \Omega)t]}{\omega + \Omega} \right\} \\ &\quad - \frac{i\omega}{2} \left\{ \frac{1 - \exp[i(\omega - \Omega)t]}{\omega - \Omega} \right\}. \end{aligned} \quad (31)$$

The last expression is formed by two terms. The first corresponds to a photon emission process, while the second represents absorption.

The squared amplitudes of the coefficients $a_{\mu\nu}(t)$ give the transition probability from state ν to state μ . At a given frequency of the electromagnetic wave Ω and considering the photon absorption mechanism, there will be two resonant frequencies, namely, (1) $\omega \approx \Omega$, which is associated with two simultaneous transitions from VB to FB and from FB to CB, and (2) $\omega \approx \Omega/2$, related to the transition from VB to CB.

Therefore, using Eq. (30) and omitting the photon emission mechanism, we obtain

$$\mathcal{P}_{2\leftarrow 1}^A = |w|^2 \frac{\sin^2[(\omega - \Omega)t/2]}{(\omega - \Omega)^2} \quad (32)$$

and

$$\mathcal{P}_{3\leftarrow 2}^A = \mathcal{P}_{2\leftarrow 1}^A \quad (33)$$

for the former case, while for the transition that does not involve the flat band

$$\mathcal{P}_{3\leftarrow 1}^A = |s|^2 \frac{\sin^2[(2\omega - \Omega)t/2]}{(2\omega - \Omega)^2}. \quad (34)$$

Hence, for transition probabilities $\mathcal{P}_{3\leftarrow 2}^A$ and $\mathcal{P}_{2\leftarrow 1}^A$ in the resonance frequency $\omega \approx \Omega$ and using the fact that $\omega = \Omega\sqrt{\kappa_x^2 + \kappa_y^2}$, we find that the maximum transitions occur when the renormalized moments satisfy $\kappa_x^2 + \kappa_y^2 \approx 1$. In Fig. 2(a), we show these transition probabilities for this resonant frequency. Similarly, for transitions $\mathcal{P}_{3\leftarrow 1}^A$ and $\omega \approx \Omega/2$, the maximum transition is given by $\kappa_x^2 + \kappa_y^2 \approx (1/2)^2$, as shown in Fig. 2(b).

V. EXACT NUMERICAL RESULTS AND DISCUSSION

In this section, we study the behavior of band occupation probabilities $|\chi_\mu(t)|^2$. To simplify the discussion, here we will focus on the particular case when the electron momentum is perpendicular to the electric field ($\theta_k = \pi/2$) and in the \mathbf{K} valley ($\xi = +1$). The results presented here are representative for other values of θ_k and for the \mathbf{K}' valley ($\xi = -1$). Then we numerically solve the system of coupled differential equations that comes from Eq. (16). For this purpose, we consider the amplitude of the electric field to have the value $E_0 = 5 \times 10^{-2}$ V/m, and the frequency of the electromagnetic wave is $\Omega = 22$ GHz. With these values and using Eq. (21), the strength parameter is $\zeta = 3.45$ GHz. In the following, we will discuss the occupation probabilities in the cases of the two resonant frequencies discussed in Sec. IV.

A. Resonance frequency $\omega \approx \Omega$: Three- and two-level Rabi problems

As we saw in Sec. IV B, one resonant frequency is at $\omega \approx \Omega$. We consider $\theta_k = \pi/2$, for which the normalized moments take the values $\kappa_x \approx 0$ and $\kappa_y \approx 1$.

In Fig. 3(a) we plot the occupation probabilities $|\chi_\mu(t)|^2$ for the VB (black line), FB (blue line), and CB (red line) for $\alpha = 1$, when the initial state is $\chi_1(0) = 1$ (numerical solution). For this value of α , the bond between sites A and B and B and C are the same (see Fig. 1). Accordingly, $\mathcal{C}_\alpha = \mathcal{S}_\alpha = 1/\sqrt{2}$. This reduces the coupling of the system of differential equations in Eq. (16) as $s = 0$. Therefore, it turns out that the matrix $\mathbb{B}(t)$ is the same as a known simplified solvable version of the three-level Rabi system [44,56] and that we can compare it with our numerical results. The main difference between the three-level and two-level Rabi systems is that the three-level one can be used to probe the medium

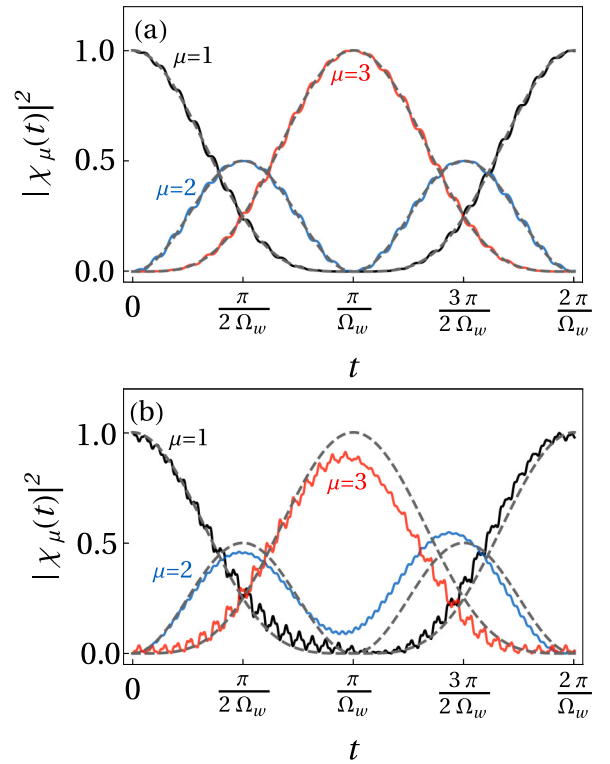


FIG. 3. Occupation probabilities $|\chi_1(t)|^2$ (black line), $|\chi_2(t)|^2$ (red line), and $|\chi_3(t)|^2$ (blue line) as a function of time for the resonant frequency $\omega \approx \Omega$. The dashed gray lines are the results obtained for the three-level Rabi problem considering only resonant terms. (a) shows the numerical results for $\alpha = 1.0$ and $\Omega_w = 1.72$ GHz. (b) shows the behavior for $\alpha = 0.2$ with $\Omega_w = 0.66$ GHz. The initial states in both panels are given by $\chi_1(0) = 1$. Note that although Ω_w is different in both panels, the periodicity is determined by Ω_w . Notice how the case $\alpha = 1$ corresponds to the three-level Rabi problem.

through the interaction with a first transition. According to Sargent and Horwitz, the band occupancies are given by [44]

$$|\chi_1(t)|^2 = \left[\cos\left(\frac{\Omega_w t}{2}\right) \right]^4, \quad (35)$$

$$|\chi_2(t)|^2 = \frac{1}{2} [\sin(\Omega_w t)]^2, \quad (36)$$

$$|\chi_3(t)|^2 = \left[\sin\left(\frac{\Omega_w t}{2}\right) \right]^4. \quad (37)$$

The band occupation probabilities present oscillations with period for the VB and CB transitions equal to $T = 2\pi/\Omega_w$, where $\Omega_w = |w|/\sqrt{2}$, with $|w|$ being defined by Eq. (19). In this particular case we have $\Omega_w = 1.72$ GHz. For the FB transitions, the oscillation period is $T/2$. The maximum amplitude of oscillations for VB and CB is equal to 1. This is a consequence of the resonant frequency and $\alpha = 1$. Notice that although the external field frequency is resonant for transitions between the FB and the cone levels, the flat state can be only half occupied. The reason is that the probability leaks from the valence band to the conduction band through the intermediate FB [44]. This can be corroborated by observing that for this case, time perturbation theory indicates that $\mathcal{P}_{3\leftarrow 1}^A = 0$, while $\mathcal{P}_{2\leftarrow 1}^A = \mathcal{P}_{3\leftarrow 2}^A$.

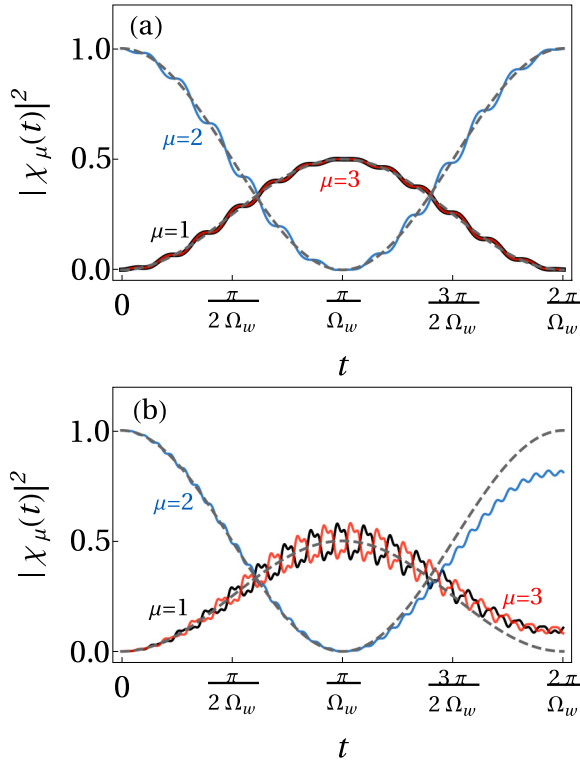


FIG. 4. Occupation probabilities $|\chi_1(t)|^2$ (black line), $|\chi_2(t)|^2$ (red line), and $|\chi_3(t)|^2$ (blue line) as a function of time for the resonant frequency $\omega \approx \Omega$. The dashed gray lines are the results obtained for the three-level Rabi problem considering only resonant terms. (a) shows the numerical results for $\alpha = 1.0$ and $\Omega_w = 3.45$ GHz. (b) shows the behavior for $\alpha = 0.2$ with $\Omega_w = 1.32$ GHz. The initial states in both panels are given by $\chi_2(0) = 1$. Note that although Ω_w is different in the two panels, the periodicity is determined by Ω_w . Notice how the case $\alpha = 1$ corresponds to the three-level Rabi problem.

In Fig. 3(a) we show a comparison between the band occupancies given by Eqs. (36)–(37) (gray dashed lines) and our numerical calculation (solid lines). We can see excellent agreement between the analytical and numerical results. However, the numerical result contains a high-frequency oscillation not seen in the Rabi solution. The reason is that right from the start, the Rabi solution considers only frequencies near resonances, as it assumes a field $V_{\text{int}}(t) = V_{\text{int}}(0)e^{i2\Omega t}$, while our numerical solution contains resonant and nonresonant frequencies.

By changing α we move away from the solvable three-level system. Figure 3(b) shows that the main effect is a change in Ω_w as w depends on α . The other effect is a reduction of the highest-band occupancy as the FB band is not empty at half period.

In twisted bilayer graphene and in the $\alpha - T_3$ graphene model, the Fermi level falls at the flat band. Therefore, it is relevant to study the system when a pure FB state is taken as the initial condition. Interestingly, in this case the three-level Rabi system mimics a two-level system due to the symmetry. This behavior is seen in Figs. 4(a) and 4(b). Figure 4(a) corresponds to the known solvable case $\alpha = 1$ in which the numerical and analytic solutions are almost the same. As we

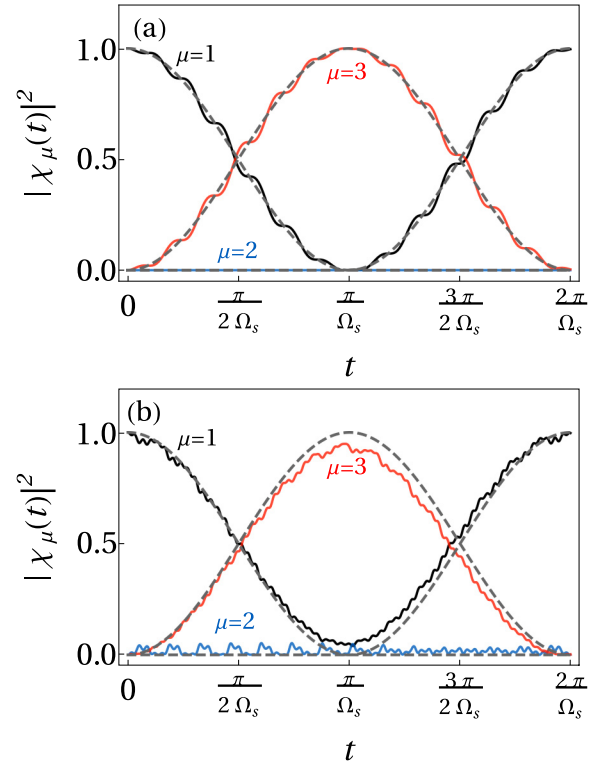


FIG. 5. Occupation probabilities $|\chi_1(t)|^2$ (black line), $|\chi_2(t)|^2$ (red line), and $|\chi_3(t)|^2$ (blue line) as a function of time for the resonant frequency $\omega \approx \Omega/2$. The dashed gray lines are the results obtained for the two-level Rabi problem considering only resonant terms. (a) shows the numerical results for $\alpha = 0.0$ and $\Omega_s = 3.45$ GHz. (b) shows the behavior for $\alpha = 0.8$ with $\Omega_s = 0.75$ GHz. The initial states in both panels are given by $\chi_1(0) = 1$. Note that although Ω_s is different in the two panels, the periodicity is determined by Ω_s . Notice how the case $\alpha = 0$ corresponds to the two-level Rabi problem.

change α , the period is modified, small ripples are observed due to nonresonant contributions, and the highest bands are never fully occupied. This suggests that upon charge doping, the system can be changed from a two- to a three-level Rabi problem.

B. Resonance frequency $\omega \approx \Omega/2$: Two-level Rabi problem

As we found in Sec. IV B, there is a second resonant frequency at $\omega \approx \Omega/2$. In Fig. 5(a) we plot the occupation probabilities for the VB (black line), FB (blue line), and CB (red line) for $\alpha = 0$, when the initial state is $\chi_1(0) = 1$. In this case, $\mathcal{C}_\alpha = 1$, and $\mathcal{S}_\alpha = 0$, and hence, the $\alpha - T_3$ lattice is a honeycomb lattice resembling monolayer graphene [25].

Hence, $w = 0$, and the matrix $\mathbb{B}(t)$ in Eq. (17) is the same as a known simplified solvable form of the two-level Rabi system [57,58]. The band occupancies are given by

$$|\chi_1(t)|^2 = \left[\cos\left(\frac{\Omega_s t}{2}\right) \right]^2, \quad (38)$$

$$|\chi_2(t)|^2 = 0, \quad (39)$$

$$|\chi_3(t)|^2 = \left[\sin\left(\frac{\Omega_s t}{2}\right) \right]^2. \quad (40)$$

The band occupation presents oscillations, where the period for the VB and CB is $T = 2\pi/\Omega_s$ and $\Omega_s = |s|$. In this particular case $\Omega_s = 3.45$ GHz. The above expressions are in agreement with the time perturbation theory presented before, where $\mathcal{P}_{2\leftarrow 1}^A = \mathcal{P}_{3\leftarrow 2}^A = 0$ and $\mathcal{P}_{3\leftarrow 1}^A \neq 0$. Such a result indicates that the FB does not contribute to the occupancy probabilities. In Fig. 5(a), we show that the numerical solution and the band occupancies (gray dashed lines), given by Eqs. (38) and (39), show excellent agreement. As in the three-level problem, the numerical result contains a high-frequency oscillation not seen in the two-level Rabi solution.

Finally, by increasing the value of α , the two-level system is difficult to solve, and the numerical solution presents two effects. As shown in Fig. 5(b), the first effect is a reduction of the highest-band occupancy in the VB and CB, and the second is a change in the frequency of Ω_s due to the shift in α in Eq. (20).

VI. CONCLUSIONS

We investigated the occupancy probabilities for the $\alpha - \mathcal{T}_3$ system under linearly polarized light by studying the corresponding Dirac equation in the interaction picture. The transitions between states have contributions that depend upon the relative angle between the electron momentum and the

electromagnetic field wave vector. When both are parallel (or antiparallel), the transitions are found by using Floquet theory, while for other directions we used time-perturbation theory and numerical solutions. This allowed us to find two resonant frequencies. The first resonance, $\omega \approx \Omega$, involves the flat band as an intermediate step (three-level system). In contrast, the second, $\omega \approx \Omega/2$, is similar to the valence and conduction band transitions observed in graphene (two-level system). The value of the parameter α plays an important role in the behavior of transitions probabilities. While for α close to 1 and $\omega \approx \Omega$ the system recovers the behavior of the three-level Rabi system, for α near zero and $\omega \approx \Omega/2$ it behaves like a two-level Rabi system. Moreover, we also showed that upon charge doping, the system can be changed from a two- to a three-level Rabi problem, unveiling many interesting possibilities for quantum control and electronic devices [59].

ACKNOWLEDGMENTS

We thank UNAM DGAPA-PROJECT IN102620. V.G.I.-S and J.C.S.-S. acknowledge the total support from a DGAPA-UNAM fellowship. M.A.M. thanks AMC for the support during the XXIV Summer of Scientific Research (2019). R.C.-B. acknowledges the hospitality of the Instituto de Física at UNAM, where this project was finished.

-
- [1] Y. Cao, V. Fatemi, S. Fang, K. Watanabe, T. Taniguchi, E. Kaxiras, and P. Jarillo-Herrero, *Nature (London)* **556**, 43 (2018).
 - [2] R. Bistritzer and A. H. MacDonald, *Proc. Natl. Acad. Sci. USA* **108**, 12233 (2011).
 - [3] U. Mogera and G. U. Kulkarni, *Carbon* **156**, 470 (2020).
 - [4] D. O. Oriekhov, E. V. Gorbar, and V. P. Gusynin, *Low Temp. Phys.* **44**, 1313 (2018).
 - [5] G. Tarnopolsky, A. J. Kruchkov, and A. Vishwanath, *Phys. Rev. Lett.* **122**, 106405 (2019).
 - [6] N. F. Q. Yuan and L. Fu, *Phys. Rev. B* **98**, 045103 (2018).
 - [7] H. L. Yu and Z. Y. Zhai, *Mod. Phys. Lett. B* **32**, 1850158 (2018).
 - [8] T. Horiguchi and C. C. Chen, *J. Math. Phys.* **15**, 659 (1974).
 - [9] B. Sutherland, *Phys. Rev. B* **34**, 5208 (1986).
 - [10] E. V. Gorbar, V. P. Gusynin, and D. O. Oriekhov, *Phys. Rev. B* **99**, 155124 (2019).
 - [11] O. V. Bugaiko and D. O. Oriekhov, *J. Phys.: Condens. Matter* **31**, 325501 (2019).
 - [12] D. O. Oriekhov and V. P. Gusynin, *arXiv:2001.00272*.
 - [13] J. D. Malcolm and E. J. Nicol, *Phys. Rev. B* **92**, 035118 (2015).
 - [14] F. Wang and Y. Ran, *Phys. Rev. B* **84**, 241103(R) (2011).
 - [15] M. Rizzi, V. Cataudella, and R. Fazio, *Phys. Rev. B* **73**, 144511 (2006).
 - [16] J. Vidal, P. Butaud, B. Douçot, and R. Mosseri, *Phys. Rev. B* **64**, 155306 (2001).
 - [17] E. Illes and E. J. Nicol, *Phys. Rev. B* **95**, 235432 (2017).
 - [18] J. Vidal, R. Mosseri, and B. Douçot, *Phys. Rev. Lett.* **81**, 5888 (1998).
 - [19] E. Illes and E. J. Nicol, *Phys. Rev. B* **94**, 125435 (2016).
 - [20] T. Biswas and T. K. Ghosh, *J. Phys.: Condens. Matter* **28**, 495302 (2016).
 - [21] A. D. Kovács, G. Dávid, B. Dóra, and J. Cserti, *Phys. Rev. B* **95**, 035414 (2017).
 - [22] T. Biswas and T. K. Ghosh, *J. Phys.: Condens. Matter* **30**, 075301 (2018).
 - [23] A. Raoux, M. Morigi, J.-N. Fuchs, F. Piéchon, and G. Montambaux, *Phys. Rev. Lett.* **112**, 026402 (2014).
 - [24] F. Piéchon, J.-N. Fuchs, A. Raoux, and G. Montambaux, *J. Phys.: Conf. Ser.* **603**, 012001 (2015).
 - [25] J. D. Malcolm and E. J. Nicol, *Phys. Rev. B* **93**, 165433 (2016).
 - [26] B. Dey and T. K. Ghosh, *Phys. Rev. B* **99**, 205429 (2019).
 - [27] H.-Y. Xu and Y.-C. Lai, *Phys. Rev. Res.* **2**, 013062 (2020).
 - [28] B. Dey and T. K. Ghosh, *Phys. Rev. B* **98**, 075422 (2018).
 - [29] A. Iurov, G. Gumbs, and D. Huang, *Phys. Rev. B* **99**, 205135 (2019).
 - [30] F. J. López-Rodríguez and G. G. Naumis, *Phys. Rev. B* **78**, 201406(R) (2008).
 - [31] F. López-Rodríguez and G. Naumis, *Philos. Mag.* **90**, 2977 (2010).
 - [32] O. V. Kibis, *Phys. Rev. B* **81**, 165433 (2010).
 - [33] H. L. Calvo, H. M. Pastawski, S. Roche, and L. E. F. F. Torres, *Appl. Phys. Lett.* **98**, 232103 (2011).
 - [34] A. E. Champo and G. G. Naumis, *Phys. Rev. B* **99**, 035415 (2019).
 - [35] V. G. Ibarra-Sierra, J. C. Sandoval-Santana, A. Kunold, and G. G. Naumis, *Phys. Rev. B* **100**, 125302 (2019).
 - [36] T. Higuchi, C. Heide, K. Ullmann, H. B. Weber, and P. Hommelhoff, *Nature (London)* **550**, 224 (2017).
 - [37] C. Heide, T. Higuchi, H. B. Weber, and P. Hommelhoff, *Phys. Rev. Lett.* **121**, 207401 (2018).
 - [38] M. Oliva-Leyva and G. G. Naumis, *2D Mater.* **2**, 025001 (2015).

- [39] M. Oliva-Leyva and G. G. Naumis, *Phys. Rev. B* **93**, 035439 (2016).
- [40] A. López, Z. Z. Sun, and J. Schliemann, *Phys. Rev. B* **85**, 205428 (2012).
- [41] A. Scholz, A. López, and J. Schliemann, *Phys. Rev. B* **88**, 045118 (2013).
- [42] C. He and Z. Zhang, *Phys. Lett. A* **378**, 3200 (2014).
- [43] L. Du, Q. Chen, A. D. Barr, A. R. Barr, and G. A. Fiete, *Phys. Rev. B* **98**, 245145 (2018).
- [44] M. Sargent and P. Horwitz, *Phys. Rev. A* **13**, 1962 (1976).
- [45] F. Guinea and N. R. Walet, *Phys. Rev. B* **99**, 205134 (2019).
- [46] P. Roman-Taboada and G. G. Naumis, *Phys. Rev. B* **95**, 115440 (2017).
- [47] P. Roman-Taboada and G. G. Naumis, *Phys. Rev. B* **96**, 155435 (2017).
- [48] P. Roman-Taboada and G. G. Naumis, *J. Phys. Commun.* **1**, 055023 (2017).
- [49] H. L. Calvo, J. S. Luna, V. Dal Lago, and L. E. F. Foa Torres, *Phys. Rev. B* **98**, 035423 (2018).
- [50] J. J. Sakurai and E. D. Commins, *Modern Quantum Mechanics* (Addison-Wesley, New York, 1995).
- [51] J. H. Shirley, *Phys. Rev.* **138**, B979 (1965).
- [52] D. A. Abanin, W. De Roeck, and F. Huveneers, *Phys. Rev. Lett.* **115**, 256803 (2015).
- [53] P. Bordia, H. Lüschen, U. Schneider, M. Knap, and I. Bloch, *Nat. Phys.* **13**, 460 (2017).
- [54] D. A. Abanin, W. De Roeck, W. W. Ho, and F. Huveneers, *Phys. Rev. B* **95**, 014112 (2017).
- [55] S. A. Weidinger and M. Knap, *Sci. Rep.* **7**, 45382 (2017).
- [56] B. W. Shore and J. Ackerhalt, *Phys. Rev. A* **15**, 1640 (1977).
- [57] I. I. Rabi, *Phys. Rev.* **51**, 652 (1937).
- [58] T. Dittrich, P. Hänggi, G.-L. Ingold, B. Kramer, G. Schön, and W. Zwerger, *Quantum Transport and Dissipation* (Wiley-VCH, Weinheim, 1998), Vol. 3.
- [59] G. G. Naumis, M. Terrones, H. Terrones, and L. M. Gaggero-Sager, *Appl. Phys. Lett.* **95**, 182104 (2009).